American Mineralogist, Volume 62, pages 13–30, 1977

Stability of Fe–Mg amphiboles with respect to sulfur fugacity

ROBERT K. POPP,[1] M. CHARLES GILBERT AND JAMES R. CRAIG

Department of Geological Sciences
Virginia Polytechnic Institute and State University
Blacksburg, Virginia 24061

Abstract

Equilibria between Fe–Mg amphiboles and pyrrhotites have been determined in the presence of magnetite and quartz at 2 kbar and 650°, 675°, 700°, 725°C. The assemblages produced may be expressed as the simultaneous equilibria:

$$\text{amphibole} + O_2 \rightarrow \text{magnetite} + \text{quartz} + H_2O \quad (1)$$

$$\text{amphibole} + S_2 \rightarrow \text{pyrrhotite} + \text{quartz} + H_2O + O_2 \quad (2)$$

At 700°C, amphiboles of 29, 41, 49, and 57 mole percent Fe end-member coexist with pyrrhotites of N ($2 \times$ atomic fraction Fe) = 0.928, 0.934, 0.943, and 0.950, respectively. Compositions of coexisting amphibole–pyrrhotite pairs apparently are not seriously affected by temperature over the range investigated, although scatter of the amphibole data does not allow a rigorous analysis. Sulfur fugacity for runs was determined from pyrrhotite compositions, while f_{O_2} was known from an experimentally determined magnetite–pyrrhotite curve. Knowledge of these two fugacities allowed calculation of fugacities of all species, including H_2O, assuming an H–O–S vapor, and thus reactions (1) and (2) were located in terms of f_{O_2} and f_{S_2}.

Several models for the amphibole solid solution were used to explain the variation in composition of coexisting amphibole–pyrrhotite pairs at 700°C. The precision of measurement of both the amphibole compositions and the fugacities of volatile species does not justify other than an ideal solution model. A standard-state enthalpy of formation of ($H^0_{298\,°;1\,atm}$) of $Fe_7Si_8O_{22}(OH)_2$ amphibole from the elements of −2262 kcal/mole was calculated from a log K_{eq} *vs.* $1/T$ plot for reaction (1).

Application of the results is limited by the scarcity of data on natural amphibole–sulfide assemblages.

Introduction

Subsolidus sulfide–silicate equilibiria have important geological applications in regional metamorphism and emplacement of ore bodies. Studies such as those of Naldrett (1966), Fullagar *et al.* (1967), and Craig and Gilbert (1974) have shown the importance of sulfide–silicate interaction to the origins, emplacement, and metamorphism of natural sulfide ore bodies. Mallio and Gheith (1972) have presented textural evidence that shows such interactions to be operative during regional metamorphism of S-rich sediments. Field investigations of the type undertaken by Guidotti (1970) provide the basis for speculation on the composition of the S-containing volatile phase during metamorphism. Carpenter (1974) has mapped a pyrrhotite isograd which roughly parallels silicate isograds, and Mohr (1972) has suggested that the kyanite isograd may be shifted to lower metamorphic grade by the preferential fractionation of iron into sulfide relative to silicates.

Early experimental studies of Kullerud and Yoder (1963, 1964) suggested the applicability of experimental techniques to the understanding of low pressure sulfide–silicate reactions. Although the majority of the experimental studies have been concerned with the qualitative aspects of sulfidation reactions, several quantitative studies of coexisting sulfide–silicate assemblages have been published. Clark and Naldrett (1972) reported equilibrium compositions of coexisting Fe–Ni olivines and Fe–Ni monosulfide solid solutions. Naldrett and Brown (1968), Hammarback and

[1] Present address: Geophysical Laboratory, 2801 Upton St., N.W., Washington, D.C. 20008.

Lindqvist (1972), and Popp and Gilbert (1974) have experimentally determined compositions of pyrrhotites coexisting with pyroxenes, biotites, or amphiboles, respectively. This paper presents the results of an experimental study of the effect of sulfur fugacity on $Mg_7 \ldots Fe_7Si_8O_{22}(OH)_2$ amphiboles. The qualitative effects of sulfidation and equilibrium amphibole–pyrrhotite compositions have been determined at P_{H_2O} = 2 kbar in the range 650° to 750°C.

Calculated sulfide–silicate equilibria

The basic thermodynamic and phase equilibria principles of importance to sulfide–silicate studies can be elucidated by considering the calculated phase relations of an Fe–Mg silicate solid solution (Mg–Fe orthopyroxenes in the brief discussion below) for which sufficient thermodynamic data are available. Figure 1 shows the calculated stability field of the Mg–Fe orthopyroxene solid solution in terms of oxygen and sulfur fugacity at 980°C and 1 atm. These T–P conditions were chosen because the calculated coexisting pyrrhotite–pyroxene compositions can then be compared with the experimental data of Naldrett and Brown (1968). The reactions representing pyroxene oxidation

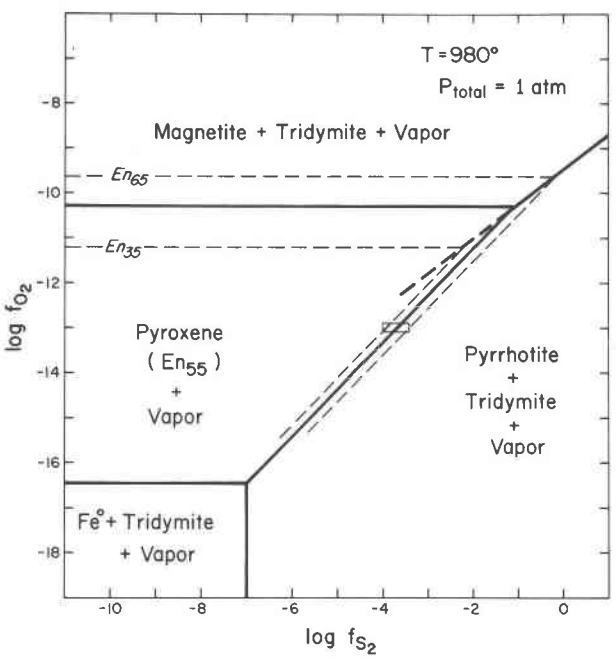

Fig. 1. Calculated phase relations for $MgSiO_3$–$FeSiO_3$ orthopyroxenes. Compositions expressed as mole percent $MgSiO_3$. Solid line equals 55 mole percent. Shaded bar represents error in determination of log f_{S_2} using the method of Toulmin and Barton (1964).

Table 1. Sources of error in calculated orthopyroxene-pyrrhotite equilibrium

Source	Error in po Composition (N)
opx composition (± 2 mole % $FeSiO_3$)	±0.002
po composition	±0.003
temperature ±20°C	±0.002
tabulated G° values ±1% error	±0.007

$$6FeSiO_3 \text{ (in pyroxene)} + O_2 \rightarrow 2Fe_3O_4 + 6SiO_2 \quad (1)$$

and sulfidation

$$2FeSiO_3 \text{ (in pyroxene)} + S_2 \rightarrow 2FeS + 2SiO_2 + O_2 \quad (2)$$

can be located in terms of f_{O_2} and f_{S_2} using the thermodynamic relation:

$$\Delta G^\circ = -RT \ln K \quad (3)$$

where ΔG° is the standard-state Gibbs free energy of reaction, K the equilibrium constant, R the gas constant, and T the absolute temperature. Standard-state free-energy values of tridymite and magnetite (assumed to be pure phases) were obtained from Robie and Waldbaum (1968); that of pyrrhotite from Barton and Skinner (1967); and that of $FeSiO_3$ was calculated by the method described by Froese (1971) utilizing Lindsley's data (1967). Assuming the pyroxene solid solution to be ideal at 980°C (*e.g.*, Navrotsky, 1971) and using the relation between sulfur fugacity (f_{S_2}), activity of FeS in pyrrhotite (a^{po}_{FeS}), and pyrrhotite composition (N = 2 × atomic fraction Fe) as determined by Toulmin and Barton (1964), the stability field of any given pyroxene composition can be calculated. The calculated stability fields of several compositions expressed as mole percent $MgSiO_3$ are shown in Figure 1. The point of intersection of reactions 1 and 2 represents the equilibrium assemblage pyroxene + pyrrhotite + magnetite + tridymite (quartz actually reported) + vapor, which is that determined experimentally by Naldrett and Brown (1968). The calculated pyrrhotite composition (N = 0.954) coexisting with pyroxene En_{55} is in fair agreement with the experimental value of N = 0.944. Table 1 summarizes the errors involved in the experimentally determined and calculated equilibria.

Two factors concerning experimental techniques for sulfide–silicate investigations are evident from Figure 1. First, because f_{O_2} is as critical a variable as f_{S_2} in determining coexisting silicate-pyrrhotite compositions, knowledge of f_{O_2} during experimental runs is essential. Second, a typical error in measurement of pyrrhotite composition using the method of Toulmin and Barton (1964) shown by the shaded bar in Figure 1 represents approximately ±30 mole percent in

pyroxene composition at the f_{S_2} and f_{O_2} values shown. Thus, a series of runs at varying f_{S_2} but constant f_{O_2} such as that imposed by standard solid-buffer techniques (Huebner, 1971) might not yield pyrrhotite compositions precise enough to be of practical value. For this reason, and additional reasons to be discussed below, standard solid-buffer techniques are not sufficient in sulfide–silicate experimental studies.

Experimental procedures

Solid starting materials for all runs were crystalline natural or synthetic phases prepared as follows:

(1) Amphiboles: synthesized to yields of >95 percent as discussed by Popp *et al.* (1976).
(2) Pyrrhotite and pyrite: synthesized from 99.999+ iron sponge (reduced with H_2 at 700°C) and sulfur in standard evacuated silica glass tubes.
(3) Magnetite: crystallized from Fisher reagent grade Fe_3O_4 + H_2O at 700°C, 2 kbar in sealed Au capsules.
(4) Quartz: Lake Toxaway quartz; crushed, sieved, acid treated.
(5) Sulfur: ASARCO, 99.999 pure.

Appropriate proportions of the above were weighed, mixed together in an agate mortar for several minutes, and then loaded into capsules along with a measured amount of distilled water.

All runs were carried out in the hydrothermal systems previously described in Popp *et al.* (1976), in which temperature and pressure were held constant to ±3°C and ±25 bars during runs. At the termination of runs, bombs were quenched at pressure, first in a stream of compressed air for 2–3 minutes, and then by immersion in water. In this manner, room temperature was reached within a maximum of five minutes.

The composition of capsule materials is an important consideration for runs in which the charge contains sulfur. Figure 2 is a log f_{S_2} *vs.* T plot at 1 atm of several relevant sulfidation curves calculated from the data of Barton and Skinner (1967). Shown as solid lines are curves for the equilibria Pt–PtS, Ag–Ag_2S, Fe–FeS, $Fe_{1-x}S$–FeS_2, and $Ag_{70}Pd_{30}$–Ag_2S assuming a_{Ag}^{AgPd} = 0.7. The dashed lines indicate pyrrhotite composition (N) as a function of f_{S_2} and T as determined by Toulmin and Barton (1964). It is obvious that several types of standard noble metals will not be suitable capsule materials for assemblages containing pyrrhotite more sulfur-rich than N of approximately 0.970. Several preliminary runs containing the assemblage amphibole + troilite (N = 1.0) + iron + H_2O were carried out in Ag capsules surrounded by the

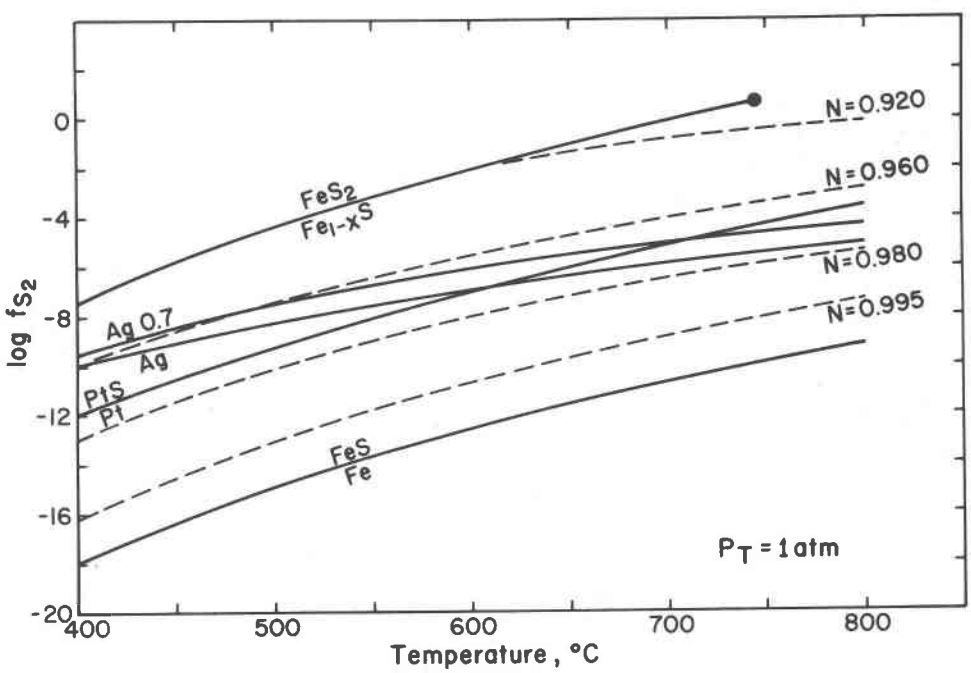

Fig. 2. Pertinent sulfidation curves calculated from the data of Barton and Skinner (1967). Dashed lines indicate pyrrhotite composition as a function of f_{S_2} and T (Toulmin and Barton, 1964).

standard solid-buffer assemblages. The capsules were badly corroded after runs, and Ag_2S was identified in the charge. Formation of Ag_2S was attributed to the oxidation of troilite and subsequent sulfidation of Ag due to an initial relatively high f_{O_2} generated by the dissociation of H_2O at the T and P of the runs.

Although the effect of increased pressure is to shift all of the curves in Figure 2 to higher f_{S_2} by small but different amounts, the magnitude of this shift is not large enough to effect the above discussion. As a result, Au capsules, which are essentially inert to sulfur over the fugacity range investigated, were used for all runs reported below. Arnold (1962) reported exchange of Au and Fe between capsules and charges consisting of pyrrhotite–pyrite assemblages to be negligible at 2 kbar between 380° and 650°C. A test run of Fe-rich amphibole at 2 kbar and 700°C showed no loss of Fe to the capsule from the silicate.

Phase identification and characterization

All runs were opened immediately after quenching, checked for the presence of water, and X-rayed immediately thereafter. Charges were examined with the petrographic microscope, with the reflecting microscope using standard polished sections, and by X-ray powder diffraction.

Amphiboles occurred as needle-like crystals averaging approximately 1–2μ by 10–15μ, often intergrown in large fibrous clumps. In some cases, a slight decrease in average grain size between reactant and product was noted. Compositions were obtained using the X-ray determinative curves discussed by Popp *et al.* (1976). Peak centers were located at 2/3 peak height on two oscillations (4 scans) run at 0.5° 2θ/minute, using synthetic spinel $MgAl_2O_4$ (a = 8.0831 Å) as an internal standard. In most runs, amphibole constituted so small a proportion of the charge that only the 440 peak could be measured precisely. Compositions determined in this manner are assumed to be accurate to ±4 mole percent Fe end-member. In a few runs, a small percentage (~ <5%) of the amphiboles were observed to have inclined extinction up to 10°. These amphiboles were confined to runs with an initially high f_{S_2}, or in double-charge runs, to the initially S-rich end of the capsule. This was interpreted as indicating inversion of a portion of the orthoamphibole to a monoclinic form as a result of breakdown at high f_{S_2}. Since the total percentage of monoclinic amphibole in the charge was small and the molar volumes (*i.e.*, unit-cell parameters) of the synthetic orthoamphiboles are roughly equivalent to the natural $C2/m$ monoclinic amphiboles, it is assumed that the determinative curves will still reflect the appropriate composition of these mixtures of the two types.

Pyrrhotite was identified by X-ray and reflected-light methods and occurred as roughly equant anhedral to subhedral grains ranging in size from 40μ down to less than 1μ. Compositions are given in terms of N_{FeS} and were determined by the location of the 102 peak (Toulmin and Barton, 1964) based on 3 oscillations (6 scans) run at 0.5° 2θ/minute, using synthetic spinel as an internal standard. As a check for systematic interlaboratory errors, the curve of Toumin and Barton was tested against and found to be consistent for four synthetic pyrrhotites of known composition. Since oxidation of fine-grained pyrrhotite in air can significantly affect d values, pyrrhotites were X-rayed immediately upon opening. However, no systematic shifts in composition were noted during X-ray scanning of a single sample for periods of up to two hours. Pyrrhotite compositions reported are assumed accurate in N_{FeS} to ±0.003. Temperatures of all runs were within the stability field of high-temperature hexagonal pyrrhotite, and quenching rates were apparently rapid enough so that the complication of low-temperature transitions was avoided. Splitting of the 102 peak, which would indicate presence of monoclinic pyrrhotite, was not observed.

Equilibrium sulfur fugacity was not high enough to yield pyrite as a stable phase in any runs reported. However, in several runs in which pyrite was a starting material, small (~3μ) equant grains of pyrite were identified optically in minor amounts (<1% total charge). The final pyrrhotite compositions in these runs were close to the pyrrhotite–pyrite solvus, and pyrite was interpreted as a metastable residuum. Arnold (1962) reported that sulfur-rich pyrrhotites quenched from temperatures higher than 650°C were found to exsolve pyrite regardless of the quenching rate. Contrary to that report, no exsolved pyrite was observed in polished sections of any runs of this study.

Magnetite was observed only in runs to which it was added as starting material. It occurred as semi-equant anhedral to subhedral grains ranging in size from 20μ to <1μ. In a number of runs, it occurred as small blebs within large pyrrhotite grains and represented residual magnetite surviving after the replacement of a larger magnetite grain by pyrrhotite. Except for such grains, no reaction rims of pyrrhotite or

magnetite were observed. The d_{400} values of several magnetites coexisting with pyrrhotite, amphibole, and quartz were measured and found consistent with those given in the ASTM file (card 11-614), and thus solution of Mg in magnetite is assumed to be minor.

Several distinct forms of quartz were observed optically in run products. Lake Toxaway quartz, added to runs to serve as a source of SiO_2, was observed as large (20μ–30μ) equant anhedral grains, whereas SiO_2 formed as a product of the sulfurization reaction occurred both as small anhedral grains down to $<1\mu$, and as doubly-terminated prisms up to $20\mu \times 5\mu$.

Talc was identified primarily from X-ray scans. It occurred as clumps of small shred-like grains roughly 1μ or smaller in size. When dispersed, it was very difficult to distinguish optically from very fine-grained quartz.

Experimental results

Preliminary sulfidation runs

Prior to attempting reversed equilibrium runs, preliminary runs were carried out in order to determine the qualitative effects of sulfur fugacity on the synthetic amphiboles as well as rates of the sulfidation reactions.

Elemental sulfur, 10–15 weight percent distilled H_2O, and synthetic amphiboles ranging in composition from 14.3 to 71.3 mole percent Fe end-member were loaded into 0.120″ O.D. Au capsules, placed within the standard FMQ buffer assemblage in large Au tubes, and run at 2 kbar in the range 650°–750°C for up to 3 weeks. Some of the inner, charge-containing capsules were welded shut, some were merely crimped shut, and others left uncrimped. Upon opening, the capsules were carefully examined. Capsules of all three types were often considerably puffed after runs, and the smell of H_2S was detected when capsules were pierced, indicating that all three types were effectively sealed during runs. A hard plug of sulfurized buffer material (magnetite, pyrrhotite, and quartz) was found in the open end of the unsealed and crimped capsules, and apparently had effectively prevented full equilibration of the vapor between inner and outer capsules.

In all runs at 700°C, regardless of starting amphibole composition, amphibole + pyrrhotite + quartz were the only products identified. Talc was present in all runs at 650°C and pyroxene in the 750°C runs. To avoid the complicating effect of the extra silicate phases, most additional preliminary runs were carried out at 700°C.

The results of a number of 700°C runs in inner Au capsules surrounded by FMQ buffer are shown in Figure 3. Initial and final amphibole compositions and final pyrrhotite compositions are plotted. The experimentally determined pyrrhotite composition coexisting with the assemblage FMQ is also shown by

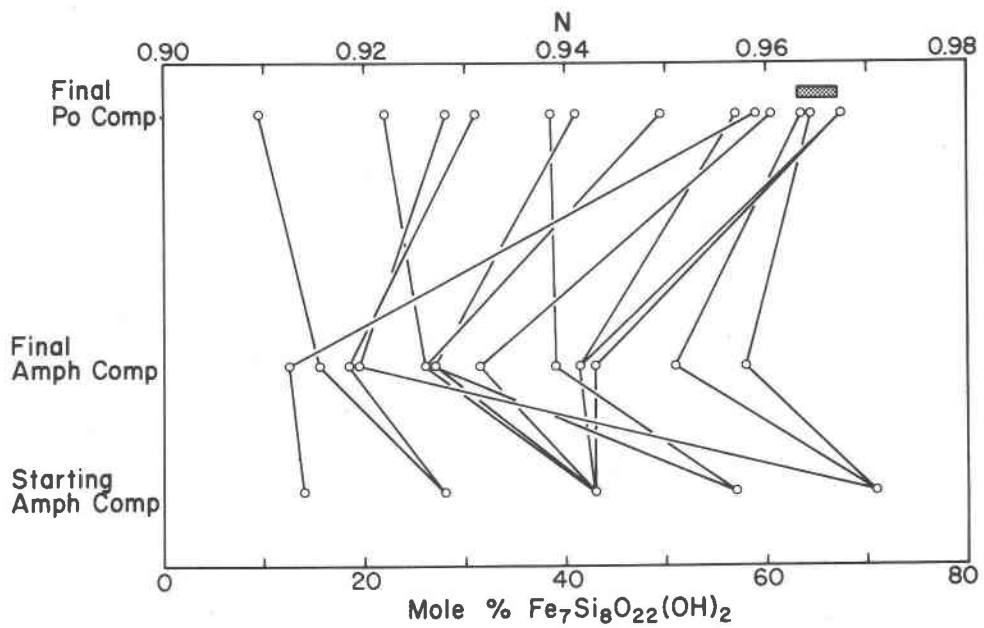

Fig. 3. Results of 700°C, 2 kbar runs starting with amphibole + sulfur + H_2O in sealed Au capsules surrounded by FMQ buffer but where effective f_{H_2} control was not maintained. Shaded area indicates experimentally determined pyrrhotite in equilibrium with FMQ at 700°C, 2 kbar, along with experimental uncertainty. See text for discussion and compare with Fig. 6.

the shaded bar (determination of this value will be discussed below). Consideration of the range of amphibole and sulfide compositions of Figure 1 suggests that f_{O_2} must vary considerably from run to run and that diffusion of H_2 through the Au capsule cannot have achieved equilibrium conditions. These runs, however, are of value in characterizing the sulfidation reaction at 700°C and 2 kbar which proceeds by the reaction:

$$[Fe_7Si_8O_{22}(OH)_2] \text{ in Fe-Mg amphibole} + 7/2\ S_2 \rightarrow 7[FeS] \text{ in pyrrhotite} + 8SiO_2 + 7/2\ O_2 + H_2O \quad (4)$$

with equilibrium constant:

$$K = \frac{(a^{po}_{FeS})^7 (f_{O_2})^{7/2} (f_{H_2O})}{(a^{amph}_{Fe})(f_{S_2})^{7/2}} \quad (5)$$

where a_{FeS} denotes activity of FeS in pyrrhotite, a^{amph} denotes activity of $Fe_7Si_8O_{22}(OH)_2$ in amphibole, and SiO_2 is assumed a pure phase.

Since equilibration of H_2 between charge and buffer could not be achieved through Au capsules, even when capsules were initially unsealed, an alternate method was devised to equilibrate f_{O_2} between charge and buffer. Charges of amphibole + sulfur in the ratio of approximately 1 : 2 were sealed in Au capsules with 10–15 weight percent H_2O and then sealed in FMQ buffer assemblages. At the temperature of the runs, pressure exerted by the sulfur vapor is great enough to rupture the inner capsule during the first several hours of the run, thus allowing interchange between the volatile phases of the charge and the buffer. Exchange of solids between the charge and buffer is very small, but pyrrhotite is formed through sulfurization of the buffer. Oxygen fugacity in both the charge and buffer should thus be that defined by the FMQ buffer. In runs of sufficient length, the composition of pyrrhotite in both charge and buffer is identical with the experimentally-determined FMQ–pyrrhotite equilibrium composition.

Table 2. Results of runs with f_{O_2} defined by FMQ buffer using the ruptured capsule method described in text. Starting materials for all runs were amphibole (57 mole % Fe_7) + sulfur + H_2O

Duration (days)	Products*	Amph. comp. (mole % Fe, ±4)	Po comp. (N, ±0.003)
1	Py+K+Tc+A+Po+Q	53	0.932
3	Py+Tc+A+K+Q+Po	32	0.930
5	Q+A+Tc+Po+K+Py	31	0.928
7	Q+A+Po+Tc	25	0.951
11	A+Po+Q	40	0.960
17	A+(Po+Q)	54	0.964

Products listed in decreasing order of abundance. The minor Po + Q in the 17 day experiment appear to have been introduced from the outer capsule.

Abbreviations: A - amphibole, Po - pyrrhotite, Q - quartz, Py - pyrite, Tc - talc, K - keatite.

Using the ruptured capsule method, identically-prepared runs containing amphibole (57 mole percent Fe end-member) + sulfur + H_2O were run at 700°C, 2 kbar in FMQ buffer for periods of 1–17 days to determine the effect of run time on the reaction. The results of these runs are given in Table 2 and are plotted in Figure 4. The dashed line is the equilibrium composition of pyrrhotite for the assemblage FMQ-pyrrhotite at 700°C, 2 kbar. It is evident that equilibrium is not achieved in the shorter runs. Under the initially high f_{S_2}, amphibole is sulfidized to produce Fe-sulfides and talc. In runs of 11 days and longer, the metastable sulfides and silicates disappear, leaving the assemblage amphibole + pyrrhotite + quartz.

Reversed equilibrium runs

Reversed tie-lines between coexisting amphiboles and pyrrhotites were determined by single runs, using a method similar to that of Naldrett and Brown (1968) and Clark and Naldrett (1972). The configuration of sealed capsules for such runs is shown in Figure 5b. The upper portion of the capsule initially contained the assemblage Mg-rich amphibole + troilite (N = 1.0) + quartz + magnetite, the lower portion Fe-rich amphibole + pyrite + quartz + magnetite, and the center portion magnetite + quartz. Ideally, the volatile phase should equilibrate throughout the entire capsule to produce a single pyrrhotite composition in all three layers and a single amphibole compostion in the upper and lower layers. The presence of magnetite + quartz serves several purposes: first, as a source of SiO_2 and Fe, which allows amphiboles to shift to more iron-rich compositions if the equilibrium relations so dictate; secondly, as a buffer for f_{O_2} from the assemblage amphibole + magnetite + quartz; and thirdly, as a means of determination of f_{O_2} from the assemblage magnetite + po. In several runs, diffusion of H_2 into the capsule resulted in the reaction of all the magnetite + quartz to amphibole. To minimize this effect, capsules were enclosed within larger Au capsules containing the assemblage magnetite + quartz + H_2O. In such a configuration, f_{O_2} should not be drastically different on opposite sides of the inner capsule, and thus diffusion of H_2 should be minimized.

Table 3 summarizes results of this series of runs. Within the error of measurement, pyrrhotite compositions in the upper, lower, and middle (where measured) layers were identical in any single run. The

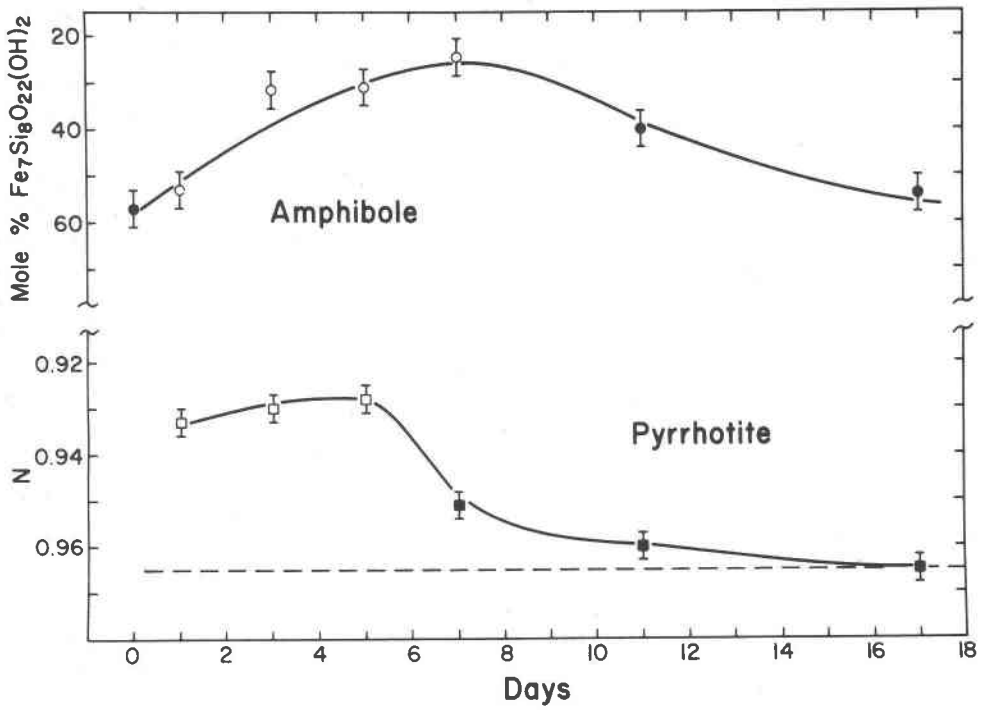

Fig. 4. Variation of amphibole and pyrrhotite compositions with time (700°C, 2 kbar, FMQ buffer). Starting materials for all runs: amphibole (57 mole percent Fe end-member) + sulfur + H_2O. Dashed line indicates equilibrium composition of pyrrhotite at FMQ buffer. Open circles indicate talc also present and open squares indicate pyrite also present.

amphiboles, however, react more sluggishly and equilibrium compositions can only be bracketed between wider limits.

In an attempt to achieve higher f_{O_2} and f_{S_2}, certain of the runs in Table 3 initially contained hematite plus quartz in the middle layer of the capsule and pyrite in both the upper and lower layers. In all such runs, magnetite + quartz was the final assemblage in the middle layer, and a single pyrrhotite composition was observed in the upper and lower layers. Even though the pyrrhotite composition has not been reversed in such runs, *i.e.*, both pyrrhotites formed from pyrite, the data of Table 3 indicate that the final composition in either half of a true reversal is the same as the reversed composition within the error of measurement.

The results presented in Table 3 illustrate four types of behavior. (i) Runs in which both the upper and lower amphiboles show significant (>4 mole percent) shift towards an intermediate composition and in which the final composition of both are within a bracket of 10 mole percent or less. These runs are considered to be good reversals, and the results of one such run are shown in Figure 5a. (ii) Runs in which both amphiboles show significant shift towards an intermediate composition with a bracket of >10 mole percent separating the final compositions. (iii) Certain runs represent only one-sided reversals, in that one amphibole showed significant reaction towards an intermediate composition but the other did not show significant reaction. (iv) The final category is that in which both amphiboles shifted in the same direction, that is, to either more Fe- or more Mg-rich compositions.

Figure 6 is a plot of product amphiboles coexisting with pyrrhotite, magnetite, and quartz at 700°C and 2 kbar. Tie lines are drawn from the centers of pyrrhotite reversal brackets to the centers of amphibole brackets for behavior type (i) and (ii) runs (solid lines). For type (iii) (dashed lines), tie lines are drawn from pyrrhotites to amphibole compositions within the reversal brackets such that the slopes are consistent with type (i) and (ii) runs. Results of type (iv) runs are not plotted.

A number of runs were made in which the middle layer initially contained iron plus quartz. In such runs lower f_{O_2} and f_{S_2} prevailed. Minor but significant amounts of olivine were observed to coexist with amphibole in the run products. At the lower f_{S_2}, overlap of the 102 pyrrhotite peak with the 400 magnetite

Table 3. Results of amphibole-sulfide runs at 2 kbar

Run #	Amphiboles[a] Starting Upper	Final Upper	Starting Lower	Final Lower	Pyrrhotite[b] Final Upper	Final Lower
			Coexisting with magnetite + quartz			
			725°C			
109	28.6	39	57.1	48	0.949	0.953
119	14.3	31	42.9	40	0.933	0.932
130	42.9	35	71.4	41	0.930	0.927
			700°C			
94	14.3	51	42.9	48	0.960	0.961
97	42.9	34	71.4	49	0.927	0.924
98	28.6	42	71.4	56	0.944	0.942
99	14.3	32	42.9	39	0.938	0.935
100	28.6	46	57.1	53	0.952	0.950
101	14.3	31	42.9	41	0.941	0.940
103	42.9	43	71.4	54	0.948	0.949
106	28.6	37	57.1	46	0.932	0.936
107	28.6	30	57.1	42	0.925	0.928
108	42.9	59	71.4	55	0.950	0.950
113[c]	14.3	26	42.9	33	0.927	0.929
131	14.3	33	28.6	36	0.952	0.953
			675°C			
111	28.6	36	57.1	41	0.937	0.937
118	14.3	31	42.9	42	0.942	0.942
126[c]	14.3	26	42.9	30	0.930	0.931
			650°C			
112	28.6	33	57.1	47	0.939	0.940
117	14.3	19	42.9	41	0.925	0.925
127[c]	14.3	23	42.9	33	0.928	0.930
			Coexisting with magnetite + quartz ± olivine + pyroxene			
			750°C			
120	14.3	30	42.9	38	0.929	0.928
			725°C			
125[c,f]	14.3	26	42.9	30	0.930	0.931
			675°C			
128[d,e,g]	42.9	49	71.4	69	0.997	
			650°C			
129[d,e,g]	42.9	55	71.4	70	0.990	
			625°C			
132[d,e]	42.9	67	71.4	77	0.959	0.959

a - *amphibole composition reported as mole % $Fe_7Si_8O_{22}(OH)_2$; ±4 for final compositions.*
b - *pyrrhotite composition reported as N; ±0.003.*
c - *runs starting with hematite plus quartz in middle layer; pyrite in upper and lower.*
d - *runs starting with iron plus quartz in middle layer.*
e - *olivine observed in run products.*
f - *pyroxene observed in run products.*
g - *overlap of 102 pyrrhotite with magnetite 400 peak; may be seriously in error. Measurement based only on pyrrhotite in middle layer.*

peak introduces serious errors into the determination of pyrrhotite compositions, shifting observed compositions to more iron-rich values. Results of these runs are reported in Table 3. All are of types (iii) and (iv) described above.

Determination of oxygen fugacity during runs

As discussed above, the presence of magnetite + quartz in equilibrium with amphibole and pyrrhotite allows determination of f_{O_2} during runs. In Figure 1, the intersections of the equilibria represented by equations 1 and 2 must lie on the curve representing the reaction:

$$Fe_3O_4 + 3/2\ S_2 \rightleftarrows 3\ FeS + 2\ O_2 \qquad (6)$$

Thus, for any given f_{S_2} (*i.e.*, pyrrhotite composition), f_{O_2} is defined, provided magnetite is present. Equilibrium f_{O_2} during the amphibole-sulfide runs can therefore be determined from an f_{O_2}-f_{S_2} plot of the magnetite-pyrrhotite equilibrium at the temperature and pressure in question. Magnetite-pyrrhotite curves were constructed in two ways.

Equation 6 allows the direct calculation of the equilibrium. $G°$ values at 1 atm for magnetite and pyrrhotite were obtained from the JANAF Tables (1971) and from Barton and Skinner (1967), respectively. $G°$ of each gas is zero by definition. Thus $\Delta G°$ at one atmosphere is known for equation 6 and K at one atm is determined by equation 3. The equilibrium constant is corrected from one atmosphere to the pressure in question (2000 bars) by the relation:

$$\ln\frac{K_2}{K_1} = \frac{-\Delta V_s}{RT}(P_2 - P_1) \qquad (7)$$

where ΔV_s is the volume of reaction of the solids, and P_2 and P_1 the pressures in question. Equation 7 follows directly from equation 3, the definition of standard states of solids and gases, and the relation

$$\left(\frac{\partial G}{\partial P}\right)_T = V \qquad (8)$$

Assuming magnetite to be a pure phase and using the relation between f_{S_2}, a^{po}_{FeS}, and N (Toulmin and Barton, 1964) also corrected to 2000 bars by equation 7, the dashed magnetite-pyrrhotite equilibrium curves at 725° and 650°C, 2 kbar, in Figure 7 were calculated. The vertical error bar on the 650° curve represents the uncertainty based on the errors in the tabulated $G°$ values.

The magnetite-pyrrhotite equilibrium was also located expermentally in following manner. When plotted in terms of f_{O_2} and f_{S_2}, the equilibria

$$3\ Fe_2SiO_4 + O_2 \rightarrow 2\ Fe_3O_4 + 3\ SiO_2 \qquad (9)$$

$$Fe_2SiO_4 + S_2 \rightarrow 2\ FeS + SiO_2 + O_2 \qquad (10)$$

also intersect to define a point on the magnetite-pyrrhotite curve at a given T and P. Oxygen fugacity of the assemblage FMQ at temperature and one atmosphere can be evaluated from the equation of Wones and Gilbert (1969) and corrected to 2000 bars by equation 7. Since f_{S_2} is defined by the pyrrhotite composition, one point on the magnetite-pyrrhotite curve is located with respect to f_{O_2} and f_{S_2} The slope of the curve is fixed by the equilibrium constant for reaction 6, *i.e.*,

$$\log K_{(6)} = 2\log f_{O_2} + 3\log a^{po}_{FeS} - 3/2\log f_{S_2} \qquad (11)$$

Reversed pyrrhotite compositions coexisting with FMQ at 2 kbar and various temperatures were ob-

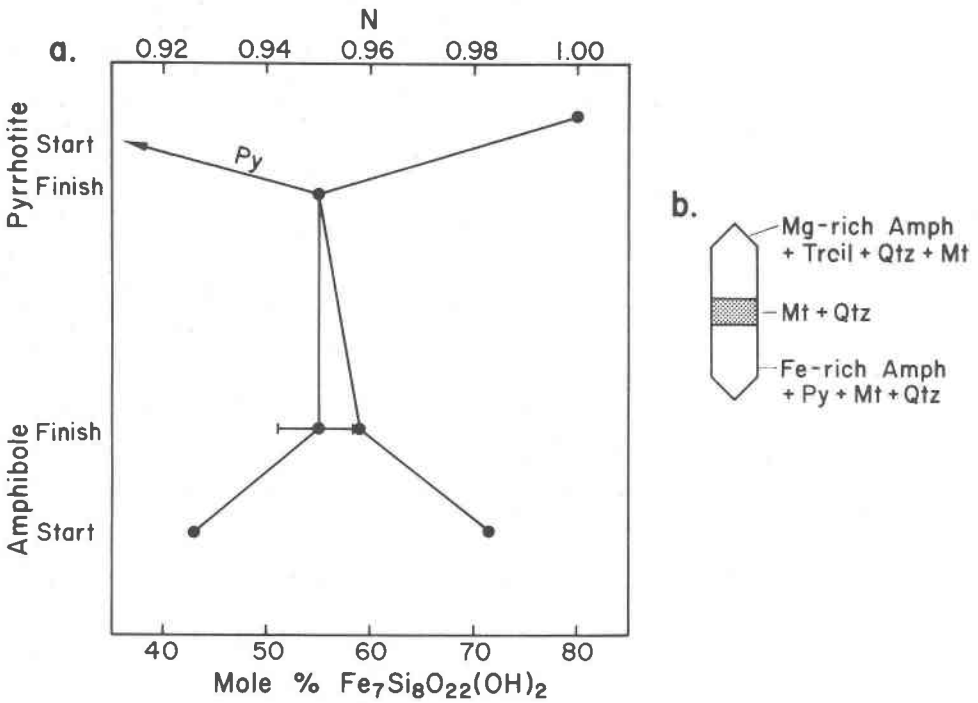

Fig. 5. a. Results of a well-reversed experiment (700°C, 2 kbar). Error bar represents uncertainty in determination of amphibole composition. b. Starting configuration of reversal runs.

tained by the double-charge capsule method used in amphibole runs. The assemblage FMQ-pyrite was contained in one end of the capsule, and the assemblage FMQ-troilite–quartz in the other. At the termination of runs, the same composition pyrrhotite plus FMQ was observed in both ends of the capsule. The results of these runs are given in Table 4. The experimental curves determined at 650°C and 725°C at 2 kbar are compared to the calculated curves in Figure 7. The horizontal error bars associated with the experimental curves represent the uncertainty in f_{S_2} based on the accuracy in measurement of N_{po}, and represent an error of roughly 0.35 log units in f_{O_2}. The experimentally determined curves were used to determine f_{O_2} in amphibole–pyrrhotite runs.

Composition of the vapor phase

Assuming negligible solubility of the solids, the vapor phase is completely defined by the H–O–S system. Possible species in the system are taken to be H_2O, H_2, O_2, S_2, SO_2, SO, H_2S, HS, and H_2SO_4. If ideal mixing is assumed, the fugacity of each species can be calculated in the manner described by Eugster and Skippen (1967). Since temperature and total pressure are known, the following equations representing equilibria between the species can be solved simultaneously for $\log f_i$:

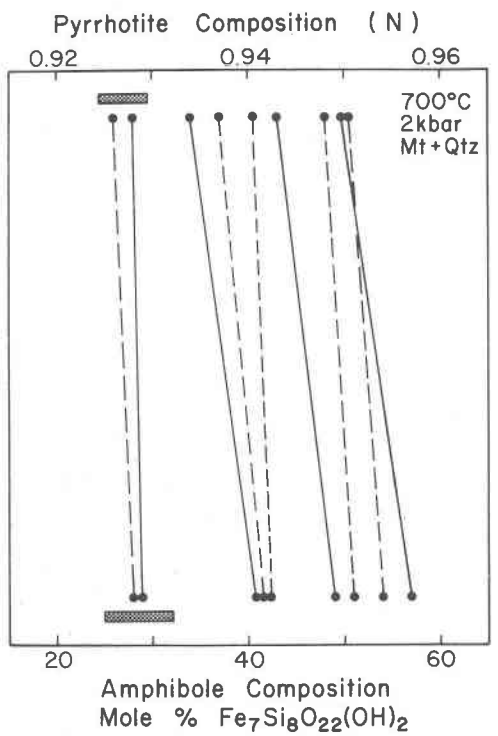

Fig. 6. Compositions of amphibole and pyrrhotite coexisting with magnetite and quartz. Run types (i) and (ii) are solid lines; run type (iii) is dashed. Error bars represent uncertainty in measurement of compositions of phases.

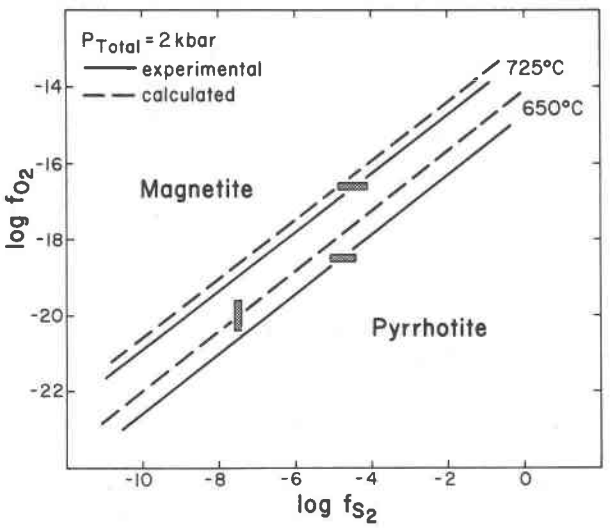

Fig 7. Comparison of calculated and experimental magnetite–pyrrhotite equilibrium. Shaded bars represent error in location.

$$P_{total} = \frac{f_{H_2O}}{\gamma_{H_2O}} + \frac{f_{H_2}}{\gamma_{H_2}} + \frac{f_{O_2}}{\gamma_{O_2}} + \frac{f_{S_2}}{\gamma_{S_2}} + \frac{f_{SO_2}}{\gamma_{SO_2}} + \frac{f_{SO}}{\gamma_{SO}} + \frac{f_{H_2S}}{\gamma_{H_2S}} + \frac{f_{HS}}{\gamma_{HS}} + \frac{f_{H_2SO_4}}{\gamma_{H_2SO_4}} \quad (12)$$

$$\log K_{H_2O} = \log f_{H_2O} - \log f_{H_2} - 1/2 \log f_{O_2} \quad (13)$$

$$\log K_{SO_2} = \log f_{SO_2} - 1/2 \log f_{S_2} - \log f_{O_2} \quad (14)$$

$$\log K_{SO} = \log f_{SO} - 1/2 \log f_{S_2} - 1/2 \log f_{O_2} \quad (15)$$

$$\log K_{H_2S} = \log f_{H_2S} - 1/2 \log f_{S_2} - \log f_{H_2} \quad (16)$$

$$\log K_{HS} = \log f_{HS} - 1/2 \log f_{S_2} - 1/2 \log f_{H_2} \quad (17)$$

$$\log K_{H_2SO_4} = \log f_{H_2SO_4} - 1/2 \log f_{S_2} - \log f_{H_2} - 2 \log f_{O_2} \quad (18)$$

$$\log f_{S_2} = x \quad (19)$$

$$\log f_{O_2} = y \quad (20)$$

where f_i's are the fugacities of the individual species, γ_i's the fugacity coefficients, K_i's the equilibrium constants for the formation of the given species, and x and y are the experimentally determined log fugacities of S_2 and O_2, respectively. Values of K_i were obtained from the JANAF Tables (1971). The fugacity coefficient of H_2O was obtained from Burnham *et al.* (1969), that of H_2 from Shaw and Wones (1974), H_2S from Ryzhenko and Vokov (1971), and that of SO_2 was estimated from the reduced variable tables of Hougen *et al.* (1964). In the range of the experimental conditions, the fugacities of the remaining species are so small that even large differences in an individual γ_i do not significantly affect the results, and therefore γ_i was set equal to unity for these species. The fugacities of O_2 and S_2 for each experimental run were determined as discussed above. Thus the fugacities of the individual species in the vapor phase coexisting with each amphibole + pyrrhotite + quartz + magnetite assemblage are known. The results for two runs at 700°C are compared below.

Table 4. Reversed fayalite–magnetite–quartz–pyrrhotite equilibria at 2 kbar

Pyrrhotite Compositions (N, ± 0.0030)					
Temp. (°C)	Upper	Lower	Average	log f_{S_2} (±0.3)	log f_{O_2} (±0.10)
725	0.9665	0.9635	0.9650	-4.48	-16.60
700	0.9650	0.9640	0.9645	-4.42	-17.27
675	0.9610	0.9610	0.9610	-4.43	-17.95
650	0.9612	0.9595	0.9604	-4.60	-18.68

	$X_{Fe}^{amph} = 0.57$, $N_{po} = 0.950$	$X_{Fe}^{amph} = 0.29$, $N_{po} = 0.928$
log f_{S_2}	−3.00	−1.24
log f_{O_2}	−16.10	−14.75
log f_{H_2O}	3.12	3.12
log f_{H_2}	0.72	0.05
log f_{H_2S}	1.51	1.72
log f_{SO_2}	−1.93	0.29
log f_{SO}	−6.18	−4.63
log f_{HS}	−4.61	−4.07
log $f_{H_2SO_4}$	−8.92	−6.02

Because amphiboles are hydrous phases, the fugacity of H_2O is an important variable in determining their field of stability. Even though it is assumed that sulfur does not enter into the amphibole structure, f_{S_2} can effect amphibole stability relations by influencing f_{H_2O} of the system as well as by direct reaction with the Fe component. Variation of f_{H_2O} at 700°C and 2 kbar total pressure is shown as a function of f_{O_2} and f_{S_2} in Figure 8. The dashed line is the magnetite–pyrrhotite equilibrium curve which was experimentally determined. Over most of the range of f_{O_2} and f_{S_2} plotted, variation of f_{H_2O} is small. However, at relatively high f_{O_2} and f_{S_2}, SO_2 becomes the dominant species in the vapor phase and f_{H_2O} is substantially decreased. At relatively low f_{O_2} and high f_{S_2} H_2S dominates the vapor phase and f_{H_2O} is again decreased.

log f_{O_2}–log f_{S_2} plot of amphibole stability

The coexisting amphibole–pyrrhotite–magnetite–quartz assemblages listed in Table 3 represent points

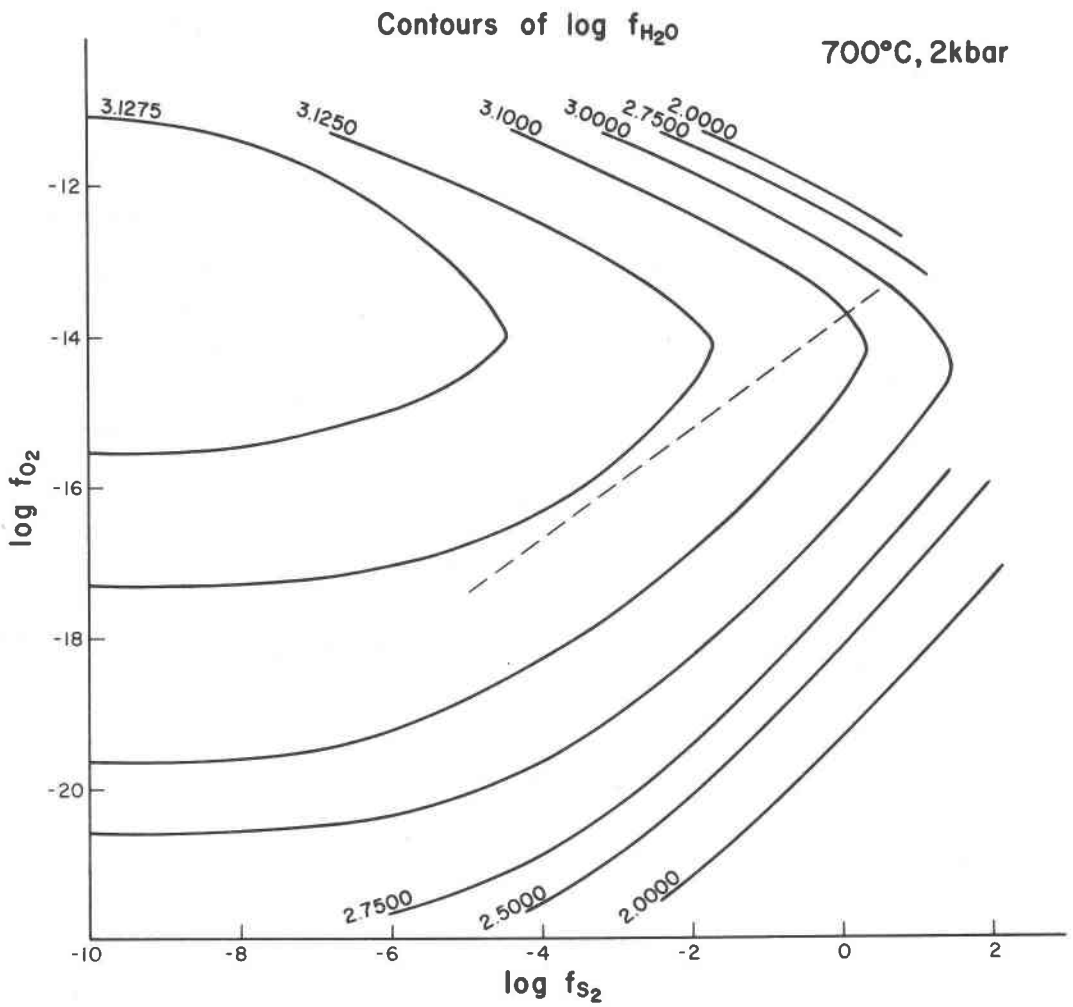

Fig. 8. Contours of calculated log f_{H_2O} in the H–O–S system at 700°C, 2 kbar. Dashed line: experimentally determined magnetite–pyrrhotite equilibrium at 700°C, 2 kbar.

that lie on the magnetite–pyrrhotite equilibrium curve in f_{O_2}–f_{S_2} space and are defined by the intersection of the following equilibria:

$$3\ Fe_7Si_8O_{22}(OH)_2 + 7/2\ O_2 \rightleftarrows 7\ Fe_3O_4 + 24\ SiO_2 + 3\ H_2O \quad (21)$$

$$Fe_7Si_8O_{22}(OH)_2 + 7/2\ S_2 \rightleftarrows 7\ FeS + 8\ SiO_2 + H_2O + 7/2\ O_2 \quad (22)$$

which represent amphibole oxidation and sulfidation, respectively. Assuming magnetite and quartz are pure phases, the log form of the equilibrium constants for (21) and (22) are given by the expressions:

$$\log K_{(21)} = 3 \log f_{H_2O} - 3 \log a_{Fe}^{amph} - 7/2 \log f_{O_2} \quad (23)$$

$$\log K_{(22)} = 7 \log a_{FeS}^{po} + \log f_{H_2O} + 7/2 \log f_{O_2} - \log a_{Fe}^{amph} - 7/2 \log f_{S_2} \quad (24)$$

Since the variation of f_{H_2O} with f_{O_2} and f_{S_2} is known, a_{FeS}^{po} is a function of f_{S_2} (Toulmin and Barton, 1964), and K_i's are constant at a given temperature, the only unknowns in (23) and (24) are the a_{Fe}^{amph} terms. It is therefore possible to extrapolate reaction (21) from the experimentally determined f_{O_2}–f_{S_2} conditions to other f_{O_2}–f_{S_2} conditions for constant amphibole composition even though the solution properties of the amphibole are not known. The extrapolation of the oxidation reaction for any amphibole composition is governed by the relation:

$$7/6\ \Delta \log f_{O_2} = \Delta \log f_{H_2O} \quad (25)$$

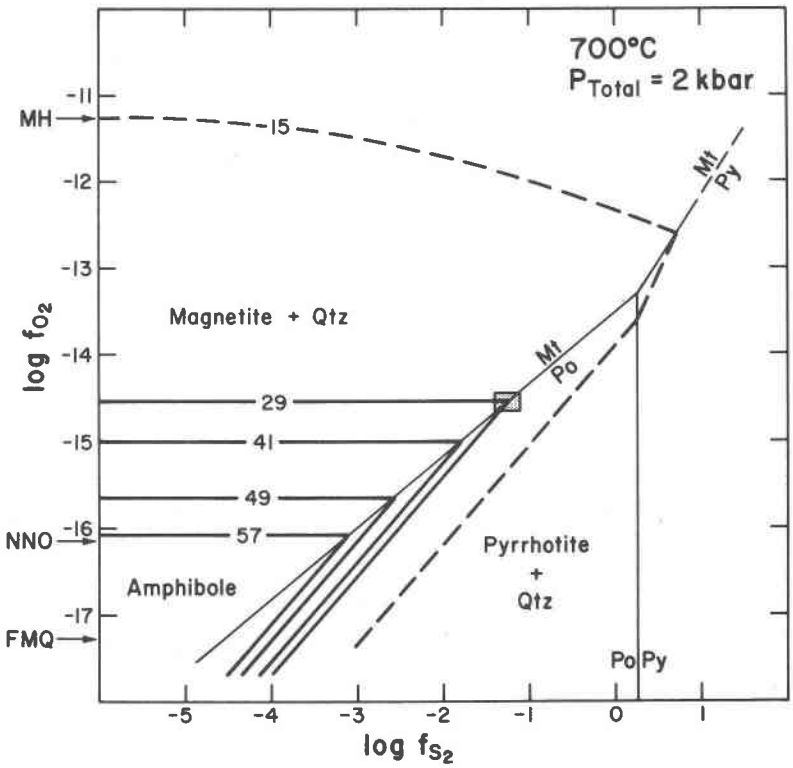

Fig. 9. Stability of amphiboles on a condensed f_{O_2}–f_{S_2} diagram. Compositions in mole percent Fe end-member. Dashed line was calculated starting from the amphibole composition determined in experiments in the S-free system. Shaded area indicates uncertainty in location of intersection. Symbols at left indicate f_{O_2} of solid buffer assemblages.

where $\Delta \log f_{H_2O}$ is the difference in $\log f_{H_2O}$ between the experimental f_{O_2}–f_{S_2} conditions and any other conditions. Similarly, for constant amphibole compositions, equilibrium (22) can be extrapolated from the experimental f_{O_2}–f_{S_2} values by the relation:

$$7\,\Delta \log a^{po}_{FeS} + \Delta \log f_{H_2O} + 7/2\,\Delta \log f_{O_2} = 7/2\,\Delta \log f_{S_2} \qquad (26)$$

Figure 9 is a $\log f_{O_2}$–$\log f_{S_2}$ plot of amphibole stability at 700°C and P_{total} = 2 kbar obtained in this manner. The stability fields of four well-reversed amphibole compositions are shown as solid lines. The shaded area represents the experimental uncertainty in location of the equilibria. The location of the pyrrhotite–pyrite equilibrium for the T–P conditions was obtained from Toulmin and Barton (1964), and the slope of the magnetite–pyrite curve was determined from the equilibrium constant for the reaction assuming pure solid phases.

The f_{O_2}–f_{S_2} conditions of the experiments lie in the range such that equilibria represented by equilibrium (21) (*i.e.*, oxidation) are only very slightly affected by f_{S_2} variations. Extrapolation of these equilibria to the lowest f_{S_2}'s in Figure 9 essentially represents amphibole stability in the S-free system. The $\log f_{O_2}$ value of -16.05 for oxidation of amphibole $X^{amph}_{Fe} = 0.57$ at low f_{S_2} is nearly identical with that of the Ni–NiO buffer (-16.16) at 700°C and 2 kbar (Huebner, 1971). The experimentally determined amphibole composition in the S-free system of 0.55 taken from Popp *et al.* (1977) is in good agreement. For the S-free system, equilibrium (21) holds for an amphibole of $X^{amph}_{Fe} = 0.15$ at f_{O_2} defined by the M–H buffer (see Popp *et al.*, 1977, Fig. 1). The dashed line in Figure 9 represents oxidation of this composition in f_{O_2}–f_{S_2}

space determined by equation 25. The effect of f_{S_2} on amphibole oxidation reactions is much more pronounced at higher f_{O_2} and f_{S_2} values.

Equilibria represented by equations 22 and 26 (*i.e.*, sulfidation) will also be affected by variation in f_{H_2O}. However, over the range of experimental conditions employed here, the effect is too small to be detectable, so that the curves representing sulfurization of amphibole are identical to those for which f_{H_2O} is constant.

Amphibole solution models

The experimental results were tested against several solution models for the Fe–Mg amphiboles. The value of $K_{(21)}$ (eqn. 23) at 700°C and 2 kbar was calculated assuming the following three different amphibole models, and then compared to an equilibrium constant obtained independent of a solution model. Because of the larger error in calculation of $K_{(22)}$, only $K_{(21)}$ was used in the comparison.

(1) Ideal solution, which assumed that Fe^{2+} and Mg^{2+} are randomly distributed over all the M sites within the amphibole structure yielding:

$$a_{Fe}^{amph} = (X_{Fe}^{amph})^7 \qquad (27)$$

$$\mu_{Fe}^{amph} = \mu^{o}{}_{Fe}^{amph} + 7RT\,ln\,X_{Fe}^{amph} \qquad (28)$$

where X_{Fe}^{amph} is the mole fraction of the Fe end-member in solution, and mixing is assumed to take place on seven cation sites within the amphibole structure.

(2) Ideal solution on the amphibole substructure (*e.g.*, Mueller, 1962; Navrotsky, 1971), which assumes Fe^{2+} to be preferentially segregated into specific structural sites but that mixing on an individual site is ideal. It was assumed that Fe^{2+} is preferentially segregated into the two $M(4)$ sites and that Fe^{2+} and Mg^{2+} are equally distributed over the two $M(1)$ sites, the two $M(2)$ sites, and the $M(3)$ site. The first assumption is consistent with previous crystal structure refinements and Mossbauer spectral studies of Fe–Mg amphiboles, and the second assumption, while not strictly correct, is probably valid considering the precision of the experimental measurements of this study. For the ideal-substructure mixing model,

$$a_{Fe}^{amph} = [X_{Fe}^{M(4)}]^2\,[X_{Fe}^{M(1)(2)(3)}]^5 \qquad (29)$$

where $X_{Fe}^{M(4)}$ is the fraction of Fe^{2+} in the $M(4)$ sites and $X_{Fe}^{M(1)(2)(3)}$ is the fraction of Fe^{2+} in the $M(1)$, $M(2)$, and $M(3)$ sites. Mueller (1962) found that such an expression gave a better approximation than an ideal solution model for empirically determined activity values of natural cummingtonites–grunerites. The variation in Fe^{2+}–Mg^{2+} distribution within the different structural sites as a function of total Fe/(Fe+Mg) ratio of the amphiboles was estimated from the data of Bancroft *et al.* (1967), Finger (1969, 1970), Ghose (1961), and Ghose and Weidner (1972). It should be noted, however, that this distribution is also a function of temperature, but that the variation of a_{Fe}^{amph} with temperature is negligible at the level of precision of the calculations.

Table 5. Comparison of log $K_{(21)}$ values at 700°, 2 kbar

	Ideal Solution	Ideal Substructure Solution	Symmetrical Regular Solution	Extrapolation to log $X_{Fe}^{amph} = 0$
Mean log $K_{(21)}$	71.31	72.41	71.61	70.06
$\hat{\sigma}$	0.74	1.45	3.90	0.84
Mean Wg			-560.	
$\hat{\sigma}$			2099.	

(3) Symmetric regular solution (*e.g.*, Thompson, 1967) in which

$$RT ln\, a_{Fe}^{amph} = 7\,RT ln\, X_{Fe}^{amph} + (1 - X_{Fe}^{amph})^2 W_g \qquad (30)$$

where W_g is an excess mixing function.

Mean values of log $K_{(21)}$ and estimated standard deviations ($\hat{\sigma}$) calculated from the 700°C data plotted in Figure 6 using the above three models to define a_{Fe}^{amph} are reported in Table 5. Using the regular solution model, the equation defining log $K_{(21)}$ contains two unknowns, log K and W_g. Thus equations from two different data points were solved simultaneously for the two unknowns. Mean W_g and the estimated standard deviation are also reported in Table 5.

A value of $K_{(21)}$ that is independent of a solution model was obtained from equation 23. The function:

$$1/21 \log K_{(21)} + 1/7 \log a = 1/21(3 \log f_{H_2O} - 7/2 \log f_{O_2}) \qquad (31)$$

(for which the right-hand side is known) was plotted against log X_{Fe}^{amph} for the same 700°C data used to calculate the equilibrium constant as just described. Linear regression analysis gave a best fit curve to the data defined by the equation:

$$1/7 \log a + 1/21 \log K_{(21)} = 0.838(0.105) \log X + 3.336(0.04). \qquad (32)$$

The slope $\simeq 1$ indicates log $X \simeq 1/7$ log a, that is, ideal solution or only slight deviation therefrom. At log $X_{Fe}^{amph} = 0$, by definition log $a_{Fe}^{amph} = 0$, and thus

1/21 log $K_{(21)}$ is defined by the intercept in equation 32. The value of log $K_{(21)}$ obtained in this manner, along with the estimated standard deviation, is also given in Table 5. Figure 10 is a plot of X_{Fe}^{amph} *vs.* $(a_{Fe}^{amph})^{1/7}$ calculated from the extrapolated value of the equilibrium constant. The data in Table 5 indicate nothing is gained beyond use of a simple ideal solution model, as all values of log $K_{(21)}$ overlap within error. Figure 10 shows a possible slight positive departure from ideality, although the uncertainties shown are *minimum* values. When the data are taken as a whole, it is concluded that the results of the present study do not justify a more elaborate model for these amphiboles than simple ideal solution.

Log K versus 1/T plots; enthalpy of formation of iron amphibole

Assuming the amphibole solution to be ideal, mean values of log K for the oxidation reaction [$K_{(21)}$, eqn. 23] and sulfidation reaction [$K_{(22)}$, eqn 24] were calculated at 725°, 700°, 675°, and 650°C from type (i), (ii), and (iii) runs (Table 3). The values are plotted against $1/T$(°K) in Figure 11. Typical errors in log K reflect the precision of measurement of f_i's and

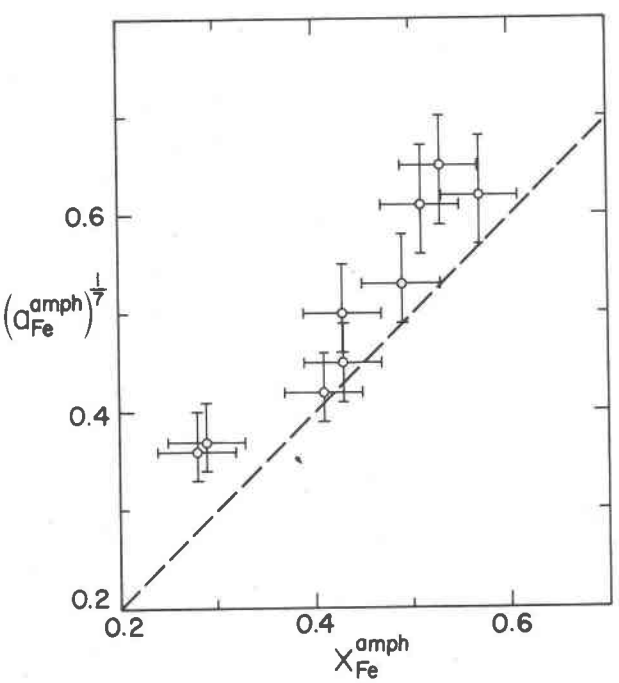

Fig. 10. Plot of $(a_{Fe}^{amph})^{1/7}$ *vs.* X_{Fe}^{amph} (700°, 2 kbar) based on the value of log $K_{(21)}$ Obtained by extrapolation to $X_{Fe}^{amph} = 1$. Uncertainty of $(a_{Fe}^{amph})^{1/7}$ represents $1\hat{\sigma}$ in log $K_{(21)}$. Uncertainty in X_{Fe}^{amph} represents minimum uncertainty in measurement of amphibole composition.

X_{Fe}^{amph}. The standard state enthalpy of reaction ($\Delta H°$) is defined by the expression:

$$\frac{d \log K}{d (1/T)} = -\frac{\Delta H°}{2.303\ R} \tag{33}$$

where R is the gas constant, and the standard state is that in which the solids are at temperature, pressure, and pure composition; the vapor at temperature and one atmosphere; and mixing of the species in the vapor phase is ideal ($H_{mix}^{\circ} = 0$). Solid lines in Figure 11 are least-squares, straight-line fits to the midpoints of the data, and the dashed lines represent maximum and minimum slopes that can be fitted through the error bars. The values of $\Delta H°$ for each set of curves are given in Table 6A. The rather large errors in determination of log K in turn result in quite large errors in $\Delta H°$ of reaction.

The value of $\Delta H°$ for each reaction was used to calculate $H°$ of formation of $Fe_7Si_8O_{22}(OH)_2$ amphibole from the elements at 298°K and 1 atm. Assuming the curves in Figure 11 to be linear down to 298°K, $\Delta H°$ at 298°K and 2 kbar is known. Values of $H°$ of formation from the elements at 298°K and 1 atm for all phases except amphibole in equations 21 and 22 were obtained from Robie and Waldbaum (1968). Values of the solids were corrected to 2 kbar by the relation:

$$\left(\frac{\partial H}{\partial P}\right)_T = V(1 - T\alpha) \tag{34}$$

where α, the coefficient of thermal expansion, was assumed to be negligible. The resulting $H°$ of formation of Fe-amphibole at 298°K and 2 kbar was then corrected to 298°K and 1 atm by equation 34. The values obtained from the midpoints of the error bars, as well as the maximum and minimum values obtained from each reaction, are summarized in Table 6B. For comparison, $H_{298,1}^{\circ}$ of formation from the elements for anthophyllite (Zen, 1971), forsterite, fayalite (Robie and Waldbaum, 1968), annite (Eugster and Wones, 1962), and phlogopite (Bird and Anderson, 1973) are also listed in Table 6B. Although the errors in the calculated $H_{298,1}^{\circ}$ for Fe-amphibole are large, the difference between its value (−2270 kcal/mole average) and that of anthophyllite (−2888.1 kcal/mole; Zen, 1971) is in the same direction as Fe and Mg end-members of other silicate solid-solution series (Table 6B). Furthermore, the differences in standard-state enthalpy of formation from the elements between the Mg and Fe end-members of the silicates noted in Table 6B, on a per

Fe atom basis, are comparable: amphibole, 89.4 kcal; biotite, 82 kcal; olivine, 83.5 kcal.

Geological applications

Amphiboles constitute major rock-forming minerals in the wall rocks of many ore bodies, especially the massive Ducktown type (Ross 1935; Kinkel 1967); thus a knowledge of sulfide–amphibole equilibria can contribute significantly to an understanding of the conditions and processes of ore formation. Sulfides and amphiboles occur together both in metamorphic terranes and in volcanogenic deposits, such as those in Newfoundland (Upadhyay and Smitheringale, 1972; Beyers, 1969). There are, however, three important factors which complicate interpretation of the ore petrology on the basis of the synthetic study described here: (1) sulfide minerals reequilibrate to temperature below 300°C on cooling and probably do not reflect the conditions of initial formation nearly so well as do the more refractory silicates: (2) the amphiboles synthesized in this study are of an undetermined structure type, unlike those in the ores; (3) the amphiboles in this study lie along the $Fe_7Si_8O_{22}(OH)_2$–$Mg_7Si_8O_{22}(OH)_2$ join, whereas the amphiboles in ores generally also contain significant amounts of Ca and Al and minor amounts of Na and K. Nevertheless, the relationships established in this study do provide insight into the far more complex chemical system represented by ore minerals and their coexistent gangue. Unfortunately, complete chemical analyses of amphiboles in association with sulfide ores are rarely reported in the literature.

Metamorphosed iron formation

Butler (1969) reported assemblages containing cummingtonite, orthopyroxene, Fe-sulfides, quartz, and magnetite from a regionally metamorphosed iron formation in the Gagnon, Quebec area. Conditions of metamorphism were estimated to be in the range 600°–700°C and 5–7 kbar. He recognized three types of assemblages on the basis of the iron sulfides present—pyrite, pyrite + pyrrhotite, pyrrhotite—but observed only small differences in the compositions of the amphiboles and pyroxenes. Fe/(Fe + Mg + Ca + Mn) for orthopyroxene varied from 0.55 to 0.57, while that for cummingtonite varied from 0.47 to 0.54. Butler suggested that the natural assemblages did not represent equilibrium. This is confirmed from the data presented in Figure 9, wherein amphibole of Fe/(Fe + Mg) = 0.18 has been calculated to coexist with pyrite + pyrrhotite + magnetite + quartz and only more Mg-rich amphibole coexists with pyrite + magnetite + quartz. If the good agreement between the calculated and experimental sulfide–orthopyroxene compositions discussed earlier also holds at lower temperatures, the analysis of Froese (1971) indicates orthopyroxene in equilibrium with pyrite + pyrrhotite must have an Fe/(Fe + Mg) ≈0.15, which is also much more Mg-rich than the reported compositions. Since sulfides are only minor constituents of these rocks, interaction between sulfides and silicates may have been limited to areas immediately adjacent to sulfide grains, in which case silicate compositions may be unaffected by sulfidation.

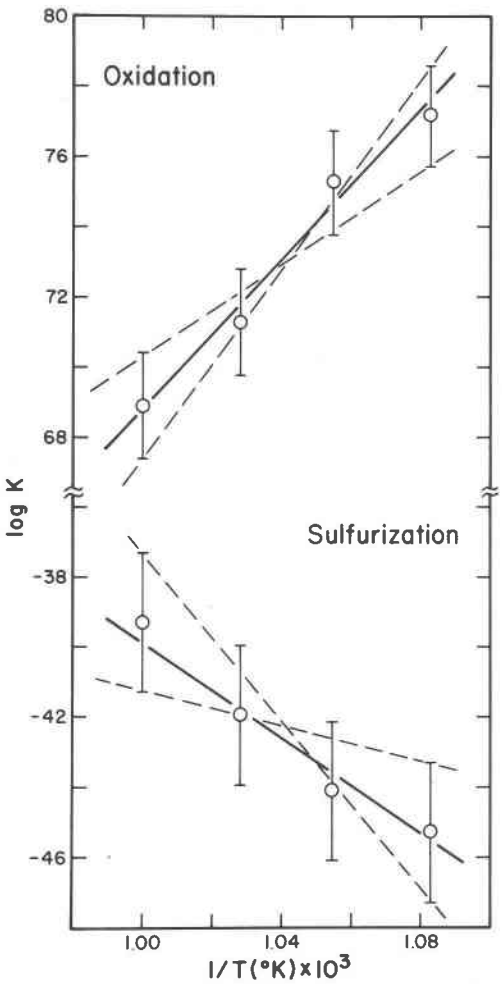

Fig. 11. Log K *vs.* $1/T$ plots for sulfidation and oxidation reactions. Solid lines: linear regression through midpoints. Dashed lines: maximum and minimum slopes which can be drawn through error bars.

Table 6A. Enthalpy of reaction (H°_r, kcal)

	Oxidation (equation 21)	Sulfidation (equation 22)
Midpoints	-482	311
Maximum	-599	529
Minimum	-295	88

Sulfide ore bodies

Froese (1969) reported cummingtonite, hornblende, and anthophyllite associated with the ore assemblage of pyrrhotite, pyrite, chalcopyrite, and minor sphalerite and magnetite at the Coronation Mine, Saskatchewan. Anthophyllite and hornblende are reported to be incompatible, but cummingtonite coexists with either. Although no spatial relations are discussed, all three amphiboles apparently coexist with sulfides in places. Values of P_{H_2O} = 2–4 kbar, T = 550°–600°C were estimated by Froese for the conditions of the final metamorphism under which the rocks from the Coronation Mine crystallized.

The Fe/(Fe + Mg) of the anthophyllite is reported in the range 0.54–0.72 determined by optical spectra. The structural formula $Fe^{2+}_{3.19}Mg_{1.97}Al_{1.22}(Fe^{3+},Mn,Ti,Ca,Na)_{0.53}Al_{1.14}Si_{6.86}O_{22}(OH)_2$ was calculated on the basis of 23 oxygens from the single complete chemical analysis given by Froese. Based on the observed assemblages, Froese (1971) has calculated the stability of amphiboles on the join Mg_5 . . . $Fe_5Al_4Si_6O_{22}(OH)_2$ with respect to f_{O_2} and f_{S_2} at 600°C and P_{H_2O} = 3 kbar. Calculated amphibole compositions coexisting with quartz, magnetite, cordierite, and pyrrhotite range from ~15 percent Fe end-member at pyrrhotite N = 0.930 to ~25 percent at N = 0.940. Even though the 600°C temperature is below the experimental range, comparison of these calculated values with experimental amphibole compositions [~28–45 mole percent $Fe_7Si_8O_{22}(OH)_2$] for the same pyrrhotite range (N = 0.93–0.94) at 650°C suggests that the iron end-member component may be destabilized by the addition of Al. It is important to note, however, that the calculations were based on a number of assumptions, including ideality of the amphibole and cordierite solid-solutions.

Craig and Gilbert (1974) reported compositions of hornblendes from both ore and unmineralized wall rock from metamorphosed massive sulfide (mostly pyrrhotite) deposits at the Gossan Lead of Virginia and Ducktown, Tennessee. Hornblendes in the ores have Fe/Mg ratios of ~0.3, whereas those from adjacent nonmineralized wall rock are in the range Fe/Mg ≥ 1.0. The estimated temperature of metamorphism at the Gossan Lead mine (~400°C, Craig *et al.,* 1971) and chemical complexity of the amphiboles again do not allow direct application of the experimental results. Furthermore it is not possible to separate the effects of host-rock bulk composition on the composition of the amphibole from those of the sulfide on the amphibole. Nevertheless the decreased Fe/(Fe + Mg + Ca) of ore amphiboles relative to non-ore amphiboles parallels the effect expected on the basis of the experimental results.

It is clear that sulfur fugacity exerts a strong control on the iron content of amphiboles. The assemblages: pyrrhotite + pyrite + magnetite and pyrrhotite + fayalite + magnetite + quartz may be taken to denote the common range of f_{O_2}–f_{S_2} conditions for amphibole occurrence. For the Fe–Mg amphiboles, the calculated corresponding range of composition at 700°C, 2 kbar, is ~18–84 mole percent Fe end-member. (For the Fe-rich compositions of this range to be stable, lower temperatures are actually required; but no appreciable error is introduced as the temperature effect on the sulfidation reaction appears negligible. See Table 3.)

In terms of present knowledge of amphibole compositions from S-rich environments, the results of this study have somewhat limited application. Although interest in silicates from these environments has increased considerably in recent years, more field and laboratory data are needed. Because of the economic importance of sulfides in massive ore bodies, additional research is needed in order to define, quantitatively and accurately, the conditions of ore formation. As is obvious from the above discussion, knowledge of the specific textural relations between opaques and silicates is necessary for meaningful in-

Table 6B. Standard state enthalpy of formation from the elements for selected silicates ($H^\circ_{298\,^\circ,1atm}$ kcal/mole)

Fe end-members	Mg end-members	Difference/atom in formula
Fe_7 Amphibole (this study)	Mg_7 Anthophyllite -2888.1 (Zen, 1971)	89.4
oxidation: midpoints -2262; max. -2223; min. -2324		
sulfidation: midpoints -2278; max. -2055; min. -2511		
Annite -1235 (Eugster & Wones, 1962) -1233.4 (Hammarbäck & Lindqvist, 1972)	Phlogopite -1482 (calculated from data in Bird & Anderson, 1972)	82.0
Fayalite -353.5 (Robie & Waldbaum, 1968)	Forsterite -520.4 (Robie & Waldbaum, 1967)	83.5

terpretation. Finally, the results of this study should serve as a starting point for additional experimental studies of more chemically complex amphiboles which have a more widespread occurrence.

Acknowledgments

The authors thank F. D. Bloss, G. V. Gibbs, D. A. Hewitt, and P. Toulmin, III, for helpful discussion and review of the manuscript. This research was supported by N.S.F. grant DES72-01587 A01.

References

Arnold, R. G. (1962) Equilibrium relations between pyrrhotite and pyrite from 325° to 743°C. *Econ. Geol., 57,* 72–90.

Bancroft, G. M., R. G. Burns and A. G. Maddock (1967) Determination of cation distribution in the cummingtonite–grunerite series by Mossbauer spectra. *Am. Mineral., 52* 1009–1026.

Barton, P. B. and B. J. Skinner (1967) Sulfide mineral stabilities. In, H. L. Barnes, Ed., *Geochemistry of Hydrothermal Ore Deposits.* Holt, Rinehart, and Winston, New York, 670 p.

Beyers, A. R. (1969) Symposium on the geology of the Coronation Mine, Saskatchewan. *Geol. Surv. Can. Pap. 68-5,* 329p.

Bird, G. W. and G. M. Anderson (1973) The free energy of formation of cordierite and phlogopite. *Am. J. Sci., 273,* 84–91.

Burnham, C. W., J. R. Holloway and N. F. Davis (1969) Thermodynamic properties of water to 1000°C and 10,000 bars. *Geol. Soc. Am. Special Pap. 132,* 96p.

Butler, P. (1969) Mineral compositions and equilibria in the metamorphosed iron formation of the Gagnon region, Quebec, Canada. *J. Petrol., 10,* 56–101.

Carpenter, R. H. (1974) Pyrrhotite isograd in southeastern Tennessee and southwestern North Carolina. *Geol. Soc. Am. Bull., 85,* 451–456.

Clark, T. and A, J, Naldrett (1972) The distribution of Fe and Ni between synthetic olivine and sulfide at 900°C. *Econ. Geol., 67,* 939–952.

Craig, J. R., C. E. Sears, M. C. Gilbert and D. A. Hewitt (1971) The Gossan Lead district, in *Guidebook to Appalachian Tectonics and Sulfide Mineralization of Southwestern Virginia,* Guidebook #5, Virginia Polytechnic Institute and State University, 25–34.

——— and M. C. Gilbert (1974) Amphiboles in Appalachian ores (abstr.) *Geol. Soc. Am. Abstr. Prog., 6,* 346.

Eugster, H. P. and D. R. Wones (1962) Stability of the ferruginous biotite, annite. *J. Petrol., 3,* 82–125.

——— and G. Skippen (1967) Igneous and metamorphic reactions involving gas equilibria. In, P. H. Abelson, Ed., *Researches in Geochemistry, Vol. 2.* John Wiley and Sons, New York 663p.

Finger, L. W. (1969) The crystal structure and cation distribution of a grunerite. *Min. Soc. Am. Spec. Pap. 2,* 95–100.

——— (1970) Refinement of the crystal structure of anthophyllite. *Carnegie Inst. Wash. Year Book, 68,* 283–288.

Froese, E. (1969) Metamorphic rocks from the Coronation Mine and surrounding area. In, A. R. Beyers, Ed., *Symposium on the Geology of the Coronation Mine, Saskatchewan. Geol. Surv. Can. Pap. 68-5,* 55–78.

——— (1971) The graphical representation of sulfide–silicate equilibria. *Econ. Geol., 66,* 335–341.

Fullagar, P. D., H. S. Brown and A. F. Hagner (1967) Geochemistry of wall rock alteration and the role of sulfurization in the formation of the Ore Knob sulfide deposit. *Econ. Geol., 62,* 798–825.

Ghose, S. (1961) The crystal structure of a cummingtonite. *Acta Crystallogr. 14,* 622–627.

——— and J. R. Weidner (1972) Mg^{2+}–Fe^{2+} order–disorder in cummingtonite, $(Mg,Fe_7)Si_8O_{22}(OH)_2$: a new geothermometer. *Earth Planet. Sci. Lett. 16,* 346–354.

Guidotti, G. V. (1970) The mineralogy and petrology of the transition from lower to upper sillimanite zone in the Oquossoc area, Maine. *J. Petrol., 11,* 277–336.

Hammarback, S. and B. Lindquvist (1972) The hydrothermal stability of annite in the presence of sulfur. *Geol. Fören. Förh., 94,* 549–564.

Huebner, J. S. (1971) Buffering techniques for hydrostatic systems at elevated pressures. In, G. Ulmer, Ed., *Research Techniques for High Pressure and High Temperature.* Springer-Verlag, New York. 367p.

Hougen, O. A., K. M. Watson and R. A. Ragatz (1964) *Chemical Process Principle Charts,* Third Edition. John Wiley and Sons, New York.

JANAF Thermochemical Tables (1971) *Natl. Stand. Ref. Data Service, Nat. Bur. Stand., 37,*1141p.

Kinkel, A. R., Jr. (1967) The Ore Knob copper deposit, N. C. and other massive sulfide deposits in the Appalachians. *U.S. Geol. Surv. Prof. Pap. 558,* 58 p.

Kullerud, G. and H. S. Yoder (1963) Sulfide–silicate relations. *Carnegie Inst. Wash. Year Book, 62,* 215–218.

——— and ——— (1964) Sulfide–silicate relations. *Carnegie Inst. Wash. Year Book, 63,* 218–222.

Lindsley, D. H. (1967) Pressure–temperature relations in the system FeO–SiO_2. *Carnegie Inst. Wash. Year Book, 65,* 226–230.

Mallio, W. J. and M. A. Gheith (1972) Textural and chemical evidence bearing on sulfide–silicate reactions in metasediments. *Mineral. Deposita, 7,* 13–17.

Mohr, D. W. (1972) *Stratigraphy, structure, and metamorphism of the eastern part of the Fontana Lake Reservoir, Great Smokey Mtns., N.C.* Ph.D. Dissertation. Department of Geological Sciences, University of Chicago, Chicago, Illinois.

Mueller, R. F. (1952) Energetics of certain silicate solutions. *Geochim. Cosmochim. Acta, 26,* 581–598.

Naldrett, A. J. (1966) The role of sulfurization in the genesis of iron–nickel sulfide deposits of the Porcupine District, Ontario. *Can. Min. Metall. Bull., 69,* 147–155.

——— and G. M. Brown (1968) Reaction between pyrrhotite and enstatite–ferrosilite solid solutions. *Carnegie Inst. Wash. Year Book, 66,* 427–429.

Navrotsky, A. (1971) The intracrystalline cation distribution and the thermodynamics of solid solution formation in the system $FeSiO_3$–$MgSiO_3$. *Am. Mineral., 56,* 201–211.

Popp, R. K. and M. C. Gilbert (1974) Sulfurization of intermediate Fe–Mg amphiboles (abstr.). *Geol. Soc. Am. Abstr. Prog., 6,* 1058.

———, ——— and J. R. Craig (1976) Synthesis and X-ray properties of Fe–Mg amphiboles, *Am. Mineral., 61,* 1267–1279.

———, ———, and ——— (1977) Effect of oxygen fugacity on the stability of Fe-Mg amphiboles. *Am. Mineral., 62,* 1–12.

Robie, R. A. and D. R. Waldbaum (1968) Thermodynamic properties of minerals and related substances at 298.15°C) and one atmosphere (1.013 bars) pressure and at higher temperatures. *U.S. Geol. Surv. Bull., 1259,* 256p.

Ross, C. S. (1935) Origin of the copper deposits of the Ducktown type in the southern Appalachian region. *U. S. Geol. Surv. Prof. Pap. 179,* 165p.

Ryzhenko, B. N. and V. P. Volkov (1971) Fugacity coefficients of

some gases in a broad range of temperatures and pressures. *Geokhimiya, 7,* 760–773 [transl. *Geochem. Int., 8,* 468–481 (1971)]

Shaw, H. R. and D. R. Wones (1964) Fugacity coefficients for hydrogen gas between 0° and 1000°C for pressures to 3000 atm. *Am. J. Sci., 262,* 918–929.

Thompson, J. B., Jr. (1967) Thermodynamic properties of simple solutions. In, P. H. Abelson, Ed., *Researches in Geochemistry, Vol. 2.* John Wiley and Sons, New York. 663p.

Toulmin, P. and P. B. Barton (1964) A thermodynamic study of pyrite and pyrrhotite. *Geochim. Cosmochim. Acta, 28,* 641–671.

Upadhyay, H. D. and W. G. Smitheringale (1972) Geology of the Gullbridge copper deposit, Newfoundland: volcanogenic sulfides in cordierite–anthophyllite rocks. *Can. J. Earth Sci., 9,* 1060–1073.

Wones, D. R. and M. C. Gilbert (1969) The fayalite–magnetite–quartz assemblage between 600° and 800°C. *Am. J. Sci., 267-A,* 480–488.

Zen, E. (1971) Comments on the thermodynamic constants and hydrothermal stability relations of anthophyllite. *Am J. Sci., 270,* 136–150.

Manuscript received, September 22, 1975, accepted for publication, September 13, 1976.